Heliyon 9 (2023) e12893

Contents lists available at ScienceDirect

Heliyon

journal homepage: www.cell.com/heliyon

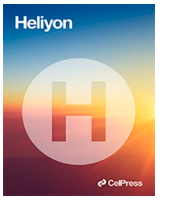

Research article

Removal of nitrides and fluorides from secondary aluminum dross by catalytic hydrolysis and its mechanism

Zhanbing Li [a,b], Huiquan Li [b,c], Xingzhong Huang [b,c], Wenfen Wu [b], Zhenhua Sun [b], Xiuwen Wu [a,*], Shaopeng Li [b,**]

[a] School of Science, China University of Geosciences Beijing, Beijing 100083, China
[b] National Engineering Research Center of Green Recycling for Strategic Metal Resources, CAS Key Laboratory of Green Process and Engineering, Institute of Process Engineering, Chinese Academy of Sciences, Beijing 100190, China
[c] School of Chemical Engineering, University of Chinese Academy of Sciences, Beijing 100049, China

ARTICLE INFO

Keywords:
Secondary aluminum dross
Catalytic hydrolysis
Aluminum nitride
Fluoride
Response surface experiment

ABSTRACT

Secondary aluminum dross (SAD) refers to hazardous waste from secondary aluminum refinement. It contains a large amount of aluminum nitride and fluorides that cause serious environmental pollution for direct discharge and hinder the resource utilization of SAD. However, it is difficult to remove nitride and fluoride simultaneously for their complicated phases. In this paper, the catalytic hydrolysis of SAD using NaOH as a catalyst to remove nitrides and fluorides synchronously was investigated systemically through single factor and response surface experiments. In addition, the chemical speciation and transformation of nitrides and fluorides were analyzed systematically. The catalytic hydrolysis removal mechanism was summarized. The optimal conditions for catalytic hydrolysis were established as follows: reaction temperature 96.60 °C; reaction time 2.85 h; liquid-solid ratio 9.28 mL/g and catalyst addition 12.62 wt %; and removal efficiency of nitrides and fluorides reached 99.03% and 81.93%, respectively. The mechanism of nitrides removal was that aluminum nitride was hydrolyzed to $Al(OH)_3$ and NH_3. NaOH reacting with $Al(OH)_3$ covering on the surface of AlN and the rapid escape of NH_3 promoted the hydrolysis of AlN under the catalysis of NaOH. The mechanism of fluorides removal was that the encapsulated fluoride particles were opened by catalytic hydrolysis to be dissolved in the solution. In this research, nitrides and fluorides were removed efficiently and synchronously. The hydrolysis residues can be used to prepare polyaluminum chloride (PAC) and ceramic materials. The hydrolysate can be prepared $NH_3{\cdot}H_2O$ by evaporative in alkaline solution. Then the solution without NH_4^+ was prepared $Al(OH)_3$ by precipitation of adjusting pH value using HCl. And the remained liquid after removing $NaAlO_2$ was used to prepare refining agent by evaporative crystallization. The work in this paper was beneficial for the utilization of SAD.

1. Introduction

The production capacity of electrolytic aluminum in China is higher than 50% of that worldwide. With the development of electrolytic aluminum in China, the annual emission of secondary aluminum dross (SAD) exceeds 4×10^6 tons [1,2]. SAD is a solid

* Corresponding author.
** Corresponding author.
E-mail addresses: wuxw@cugb.edu.cn (X. Wu), shpli@ipe.ac.cn (S. Li).

https://doi.org/10.1016/j.heliyon.2023.e12893
Received 31 July 2022; Received in revised form 5 January 2023; Accepted 6 January 2023
Available online 9 January 2023

waste of primary aluminum dross extracted aluminum, which was discharged during aluminum electrolytic, processing and regeneration [3]. When SAD contacts water, hazardous gases, such as ammonia and hydrogen, are released into the atmosphere [4]. At the same time, the dissolution of soluble salts, especially fluorides and chlorides, also cause serious-earth pollution [5]. However, SAD contains many high-value metallic oxides, such as alumina, magnesium oxide, and silica [6]. The storage or landfilling of SAD would not only restrict the development of the aluminum industry but also cause serious wastage of resources. Thus, there is an urgent need to realize the harmless treatment and resource utilization of SAD.

In recent years, various methods for utilizing SAD were reported, such as the preparation of refractory materials [7,8], ceramics [9–12], alumina [13,14], flocculating agents [15–17], cement clinker [18,19], and hydrogen [20]. However, the harmful impurities in SAD or hydrolysis residues, such as nitrides and fluorides, influence the properties of the products seriously. To avoid the effect of SAD impurities on the product performance and prevent polluting the environment, some researchers have tried to leach active aluminum from hydrolysis residue with acid or alkali, and then converted aluminum ions into different kinds of aluminum products [21–24]. However, the process is too complicated and produces a large amount of wastewater with secondary pollution, which hinders the utilization of SAD. Therefore, the complete removal of harmful impurities such as nitrides and fluorides is the key to the utilization of SAD.

At present, the common method of removing impurities from SAD is hydrometallurgy. Zhao et al. [25] proposed the method of removing fluorine, chlorine, and nitride from aluminum dross by wet process. The removal efficiency of nitride and fluorine were 62.8% and 77.6%, respectively, and the chlorine was completely removed. Lv et al. [26] investigated the effects of hydrolysis parameters on AlN content in SAD. Under optimum condition, the content of AlN in hydrolysis decreased from 12.88% to 2.25%. The removal efficiency of AlN is about 82.53%. Li et al. [27] investigated the hydrolysis behavior of AlN in the leaching of SAD using deionized water as a solvent. The results showed that AlN was easily hydrolyzed at optimum reaction temperature. The above studies are aimed at the removal of AlN by hydrolysis. However, the removal efficiency of fluorine and nitride were much lower than catalytic hydrolysis. The catalytic hydrolysis of SAD is that the product layer formed is destroyed by catalyst to promote the hydrolysis of AlN completely. In the alkali-catalyzed hydrolysis routes of disposal SAD, Li et al. [28] found that the mechanism of nitrides and fluorides removal were chemical reaction and dissolved process, respectively. The complete removal of fluorides from SAD is difficult. Shen et al. [3] summarized the alkali route of preparing γ-Al_2O_3 from SAD, which was similar to the Bayer process. Tang et al. [29] reported that the fluorides and nitrides could be removed simultaneously in combination with the Bayer process. They also proposed two stages to convert nitrides into NH_3 and insoluble fluorides into soluble fluoride by sintering with Na_2CO_3 or Na_2SO_4. However, the fluorides in SAD were dissolved into saturated sodium aluminate solution, which affects the reaction conditions of the Bayer process and increased the emission of red mud. Gao et al. [30] proposed an innovative technology to remove soluble sodium fluoride and active cryolite in alkali leaching. The leaching rate of active fluorides was 95.8% at a catalyst addition 31 wt %, leaching temperature of 80 °C, liquid-solid ratio of 4, and leaching time of 20 min. However, the consumption of NaOH was huge, and controlling the reaction of active aluminum and AlN in SAD was difficult. Lv et al. [31] studied the hydrolysis behavior of AlN in SAD using NaOH as an addition, and the optimal removal efficiencies of nitrides, chlorine, and fluorine at a leaching time of 180 min, leaching temperature of 95 °C, catalyst addition 4 wt %, and liquid to solid ratio of 6 mL/g were 96.24%, 95.63%, and 69.17%, respectively. However, the removal efficiency of fluorides is low, and the residual fluoride will influence the resource utilization of hydrolysis residue. Liu et al. [32] proposed alkali-catalytic for the removal of nitrogen and chlorine from black aluminum dross. Under optimum conditions: reaction temperature of 90 °C, reaction time of 300 min, liquid-to-solid ratio of 6 mL/g, stirring speed of 300 r/min, and particle size less than 150 mesh, the removal rate of AlN and chloride ions were 93.48% and 99.84%, respectively. Zhu et al. [33] made a feasibility analysis of the synergistic removal of nitrides and chlorines by alkali routes. The results revealed that the alkali destroyed the product layer formed by AlN hydrolysis to promote the removal of AlN and chlorines. However, the removal efficiency and mechanism of fluorides was not mentioned, which was a critical effect for the utilization of SAD. The comparison of different alkali routes were listed in Table S3.

Although catalyst hydrolysis of SAD was investigated by many authors, most researches focused on AlN removal and its mechanism. There are few reports on simultaneous nitrogen and fluoride removal and its mechanism. The interaction between factors in the process of nitrogen and fluoride removal, the possible side reactions and the effects of side reactions on fluoride and nitrogen removal have not been studied. Therefore, an innovative technology that can remove nitrides and fluorides from SAD efficiently and simultaneously is still expected.

To remove nitrides and fluorides from SAD simultaneously, a catalytic hydrolysis approach is proposed in this article. The amount of catalyst addition is strictly controlled to ensure mild reaction and high nitride and fluoride removal efficiency. The pH values of the leaching solution changed with the reaction time and the effect of factors, such as the initial pH values of the solution, reaction temperature, reaction time, catalyst addition, and liquid-solid ratio, on the removal efficiency of impurities were investigated in single-factor experiments. Subsequently, the catalytic hydrolysis conditions are further optimized by response surface experiments to achieve the efficient and simultaneous removal of nitrides and fluorides. The mechanism of catalytic hydrolysis to remove nitrides and fluorides from SAD is investigated by analyzing the mineral phase structure, chemical speciation, and chemical bonds in the catalytic hydrolysis process. The possible chemical reactions were fully analyzed to explain the removal mechanism furtherly. The catalytic hydrolysis process conditions in this paper provide a reference for the industrial disposal of SAD. The hydrolysis residues after removing nitrides and fluorides can be used to prepare polyaluminum chloride (PAC) and ceramic materials. The hydrolysate can be prepared $NH_3{\cdot}H_2O$ by evaporative in alkaline solution. Then the solution without NH_4^+ was prepared $Al(OH)_3$ by precipitation of adjusting pH value using HCl. And the remained liquid after removing $NaAlO_2$ was used to prepare refining agent by evaporative crystallization. The prepared refining agent can be used in the aluminum recovery system. The process proposed in this paper can realize the recycling of SAD and promote the healthy development of the aluminum industry.

2. Experimental

2.1. Materials

SAD was generated from an electrolytic aluminum factory in Shandong Province, China. The SAD discharged from primary aluminum dross extracted aluminum, which generated from the industry process of electrolytic aluminum water to prepare aluminum alloy. As shown in Table 1, the main components of SAD examined by X-ray fluorescence spectrometry (XRF) were Al, Mg, N, F, and Cl, and their mass fractions were 37.65%, 6.67%, 4.09%, 2.19%, and 1.73%, respectively. The phase of SAD was detected by X-ray diffractometry (XRD). As shown in Fig. 1, the main mineral phases of SAD included Al_2O_3 (PDF#88-0826), $MgAl_2O_4$ (PDF#78-1602), CaF_2 (PDF#77-2094), and AlN (PDF#75-1620). Sodium hydroxide (NaOH), boracic acid (H_3BO_3), and hydrochloric acid (HCl) were purchased from Beijing Chemical Works (Beijing, China).

2.2. Experimental design

Single-factor and response surface experiments were designed to obtain the optimum conditions for the removal of nitrides and fluorides from SAD. The single-factor experiment was completed to obtain the primary conditions that ignored the interaction of influencing factors. Subsequently, a response surface experiment was conducted, and the optimum conditions were obtained by model calculation with full consideration of the interaction among the influencing factors.

2.2.1. Single-factor experimental design

Before the single-factor experiment, the hydrolysis experiment of SAD in deionized water was carried out, and the change in the pH values of the leaching solution with reaction time was investigated at a reaction temperature of 95 °C and a liquid–solid ratio of 3 mL/g. The effect of the initial solution pH values on the removal efficiency of nitrides and fluorides from SAD at a reaction temperature of 95 °C, a reaction time of 3 h, and a liquid–solid ratio of 3 mL/g was also investigated. In single-factor experiments, when one factor was studied, the levels of other factors remained constant. Factors of reaction temperature (80 °C−100 °C), reaction time (1.5 h−3.5 h), liquid-solid ratio (3 mL/g−7 mL/g), and catalyst addition (3%–15%) were investigated. The amount of catalyst was calculated by the weight proportion of the catalyst in the total amount of SAD and catalyst.

2.2.2. Response surface experimental design

The response surface method is a statistical test design for optimizing biological processes. It is used to establish a continuous variable surface model and evaluate the factors that affect biological processes and their interactions. In this study, the experiment was set up using the Box–Behnken model to confirm the interaction of factors that affect the removal of nitrides and fluorides from SAD. Based on a single-factor experiment, four factors with reaction temperatures (A) that ranges from 70 °C to 100 °C, reaction time (B) that ranges from 1 h to 5 h, liquid-solid ratio (C) that ranges from 3 mL/g to 10 mL/g, and catalyst addition (D) that ranges from 0% to 15% were selected. The removal efficiencies of nitrides (R_1) and fluorides (R_2) were taken as the response values. The experimental factors and levels were listed in Table 2.

2.3. Analysis

The content of nitrides in SAD and hydrolysis residue was an important index tested by chemistry titration. The procedure was described as follows: (1) 1 g solid sample and 200 mL NaOH solution (20 wt%) were mixed in a 250 mL conical flask (No. 1); (2) 250 mL H_3BO_3 (2.5 wt%) was added to another conical flask (No. 2); (3) the two aforementioned conical flasks were connected by a catheter, which was extended below the level of H_3BO_3; (4) Conical flask No. 1 was heated, and the NaOH solution was kept boiling until the liquid of conical flask No. 2 reached 400 mL; (5) the liquid in conical flask No. 2 was moved to a 500 mL volumetric flask and constant volume to 500 mL; (6) a total of 100 mL solution was withdrawn and measured accurately from 500 mL volumetric flask for titration by HCl; (7) the content of nitrides was calculated using Formula 1.

$$\omega_N = \frac{C \times V \times 14}{G \times 200} \times 100\%, \tag{1}$$

where ω_N (wt. %) is the mass fraction of nitrides, C (mol/L) is the concentration of HCl, V (mL) is the consumption of HCl for the titration, and G (g) is the weight of the solid sample.

The removal efficiency of AlN was calculated by using Formula 2.

$$\eta_N = \frac{m_1 - m_2}{m_1} \times 100\%, \tag{2}$$

Table 1
Chemical composition of SAD (wt. %).

Al	Mg	Na	K	Si	Ca	N	S	Fe	Mn	Se	O	Ti	F	Cl
37.65	6.67	1.70	3.21	0.92	0.72	4.09	0.64	0.37	0.29	0.28	39.43	0.11	2.19	1.73

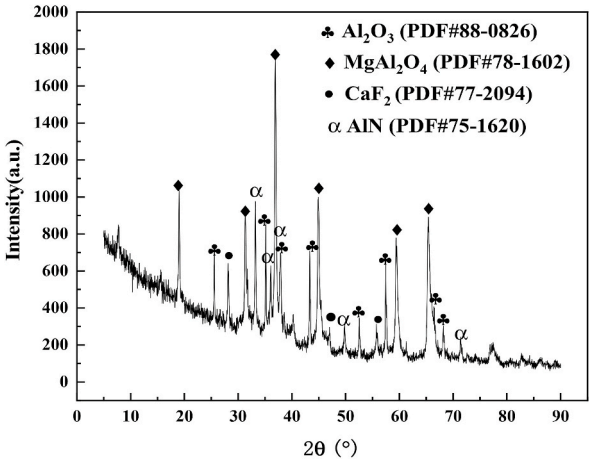

Fig. 1. XRD pattern of SAD.

Table 2
Experimental design of factors and levels.

factors	Units	Code	Code values of different levels		
			−1	0	1
Reaction temperature	°C	A	70	85	100
Reaction time	h	B	1	3	5
Liquid-solid ratio	mL/g	C	3	6.5	10
Catalyst addition	%	D	0	7.5	15

where η_N (%) is the removal efficiency of nitrides, m_1 (g) is the weight of nitrides in SAD, and m_2 (g) is the weight of nitrides in hydrolysis residue.

The content of fluorides in the solution was determined by the ion-selective electrode method (GB7484-87). The removal efficiency of fluorides was calculated by using Formula 3.

$$\eta_F = \frac{m_l}{m_s} \times 100, \tag{3}$$

where η_F (%) is the removal efficiency of F, m_s (g) is the weight of F in SAD, and m_l (g) is the weight of F in solution.

The chemical compositions of the solid samples, except for nitrides, were examined by XRF (AXIOS-MAX, 50 kV, 60 mA). The mineral phases were examined by XRD (Empyrean, CuKα, 40 kV, 40 mA) in a 2θ range from 5° to 90°. The morphology and mapping

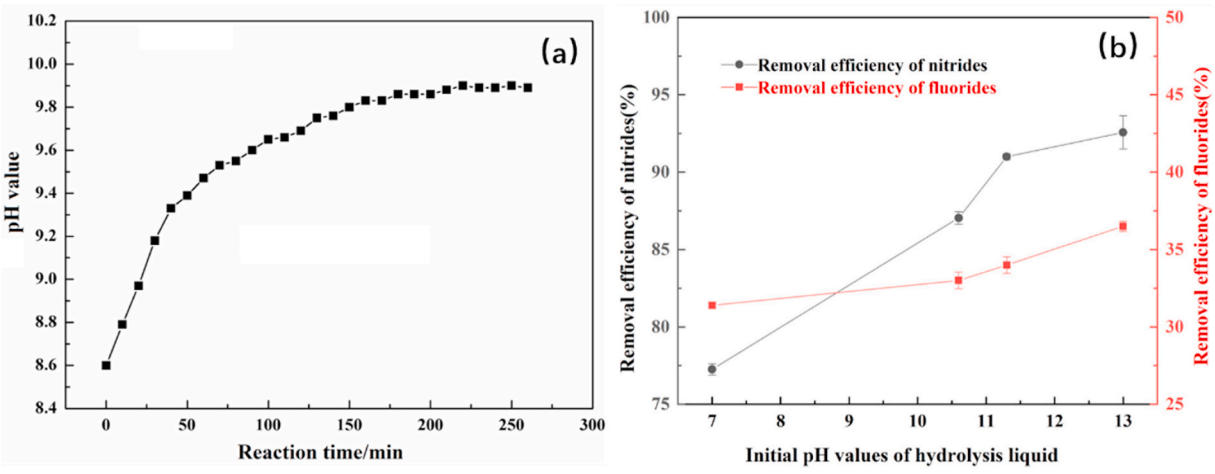

Fig. 2. (a) Changes in pH values in hydrolysis liquid with reaction time in deionized water leaching; (b) Effect of initial pH values in hydrolysis liquid on the removal efficiencies of nitrides and fluorides.

were detected by scanning electron microscopy (SEM, FEI MLA Quant 250) under the BSE model with an acceleration of 25 kV. The particle size was analyzed by a Malvern Mastersizer (Hydro 2000 MU). Fourier infrared spectroscopy (FTIR, TENSOR 27) was used to study the structural changes in the main compounds in the SAD and hydrolysis residue. N_2 adsorption and desorption (Quanta Chrome Autosorb-1) were measured to determine the pore structure. Each sample was degassed under vacuum at 573 K for 3 h before measurement. The specific surface areas were calculated from the N_2 adsorption data that ranged from $P/P_0 = 0.05$ to 0.30 according to the BET model. Pore size distributions were obtained by analyzing the desorption branch according to the Barrett–Joyner–Halenda method. X-ray photoelectron spectroscopy (XPS, ESCALAB 250Xi) was used to analyze the main element-binding form, and the results were analyzed by Thermo Scientific Avantage software according to the NIST X-ray Photoelectron Spectroscopy Database and the Handbook of X-ray Photoelectron Spectroscopy. The carbon at binder energy of 248.88 eV was used as the calibration carbon.

3. Results and discussion

3.1. Effect of initial pH values on removal efficiency

Fig. 2(a) shows the changes in the pH values in hydrolysis liquid with reaction time in deionized water leaching. The pH values in the hydrolysis liquid increased from 7 to 9.9 with the reaction time. In the hydrolysis process without an alkali catalyst, the AlN from SAD was hydrolyzed to $Al(OH)_3$ and NH_3, and ammonia disassociated OH^-, thereby increasing the pH values of the hydrolysis liquid to alkalinity. As shown in Fig. 2 (b), when the initial pH values of the hydrolysis liquid was adjusted from 7 to 13, the removal efficiency of nitrides and fluorides increased from 77% to 92.5% and 31.4%–36.5%, respectively. As the initial pH values of hydrolysis liquid rise, the removal efficiencies also showed an obvious increase. Alkali catalyst for the leaching process is beneficial for the removal of nitrides and fluorides from SAD. Therefore, investigating the effect of NaOH as a catalyst on the removal efficiencies of nitrides and fluorides is necessary.

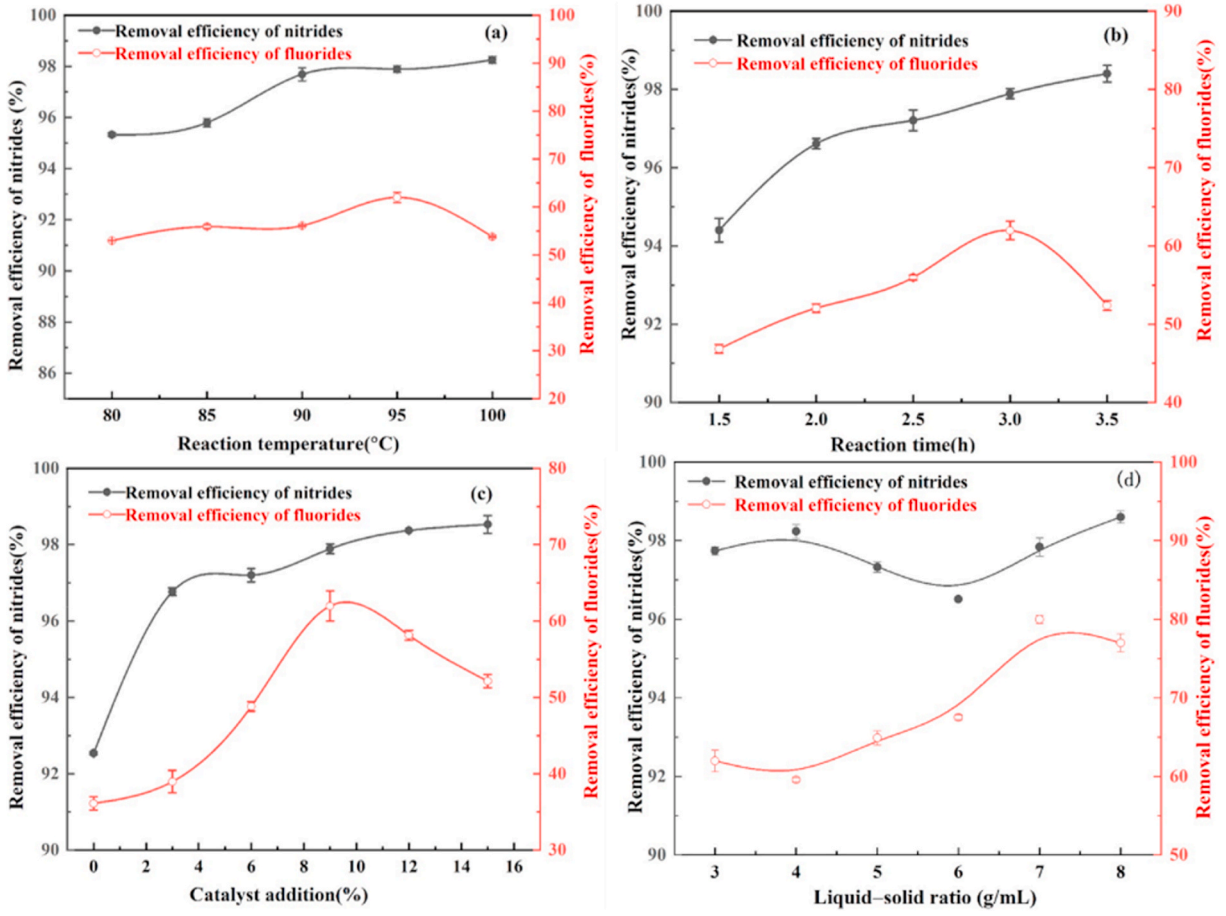

Fig. 3. Effect of different factors on the removal efficiency of nitrides and fluorides (a) reaction temperature; (b) reaction time; (c) catalyst addition; (d) liquid-solid ratio.

3.2. Single-factor experiment

3.2.1. Effect of reaction temperature on removal efficiency

Fig. 3(a) shows the effect of reaction temperature on the removal efficiency of nitrides and fluorides from SAD under a reaction time of 3 h, liquid-solid ratio of 3 mL/g, and catalyst addition of 9%. As shown in Fig. 3(a), the removal efficiency of nitrides increased from 95.33% to 98.26% as the reaction temperature increased from 80 °C to 100 °C. When the reaction temperature reached 95 °C, the removal efficiency of nitrides slowly increased. The removal efficiency of fluorides increased as the reaction temperature rose when the reaction temperature was less than 95 °C. The maximum removal efficiency of fluorides reached 61.97%. A high reaction temperature promoted the hydrolysis of AlN but consumed a large amount of water in the hydrolysis reaction, which decreased the liquid-solid ratio and was not conducive to the dissolution of fluoride. On the other hand, the concentration of $NaAlO_2$ increased with the increasing of reaction temperature, which promote to convert leached NaF and NH_4F into cryolite [34]. Reaction temperature greater than 95 °C is not conducive to removal of fluoride. The optimum reaction temperature was 95 °C.

3.2.2. Effect of reaction time on removal efficiency

The effect of reaction time on the removal efficiency of nitrides and fluorides from SAD was investigated under the following conditions: reaction temperature of 95 °C, liquid-solid ratio of 3 mL/g, and catalyst addition of 9%. As shown in Fig. 3(b), the removal efficiency of nitrides increased from 94.39% to 98.46% when the reaction time increased from 1.5 h to 3.5 h. The removal efficiency of fluorides increased and then decreased with the rising reaction time. The maximum removal efficiency of fluorides with a reaction time of 3 h was 61.97%. The removal efficiency of nitrides increased with the increasing of reaction time for the catalytic hydrolysis of AlN. At the same time, the concentration of $NaAlO_2$ and fluorides increased with the reaction time. Solution fluorides were converted to cryolite, which would remain in hydrolysis residues. The optimum reaction time was 3 h considering the synchronized removal efficiency of nitrides and fluorides.

3.2.3. Effect of catalyst addition on removal efficiency

Fig. 3(c) shows the effect of catalyst addition on the removal efficiency of nitrides and fluorides at a reaction temperature of 95 °C, reaction time of 3 h, and liquid-solid ratio of 3 mL/g. As shown in Fig. 3(c), the removal efficiency of nitrides increased from 92.53% to 98.53% as catalyst addition increased from 0% to 12%. The removal of fluorides reached 61.97% when a 9% catalyst was added. When the catalyst addition was more than 9%, the removal of fluorides began to decrease from 62.00% to 52.13%. The main reason was that catalyst NaOH destroyed the coating formed by the hydrolysis of AlN. The removal efficiency of nitrides increased with catalyst addition. However, the reactant of $NaAlO_2$ reacted with fluoride salts to form cryolite precipitation, resulting in a decrease in fluoride

Table 3
Analysis results of response surface experiments.

Experimental No.	*A*/°C	*B*/h	*C*/mL/g	*D*/%	R_1 (Removal efficiency of nitrides)/%		R_2 (Removal efficiency of fluorides)/%	
					actual	Calculated	actual	Calculated
1	85	1	3	7.5	91.21	90.50	52.55	52.73
2	70	3	6.5	15	88.95	97.94	51.31	52.42
3	70	1	6.5	7.5	81.75	72.10	51.88	51.50
4	85	3	6.5	7.5	95.71	96.34	60.97	68.39
5	100	1	6.5	7.5	98.34	91.59	68.92	66.77
6	85	1	6.5	0	26.62	39.93	8.08	7.59
7	100	3	6.5	15	94.09	87.54	66.58	64.54
8	70	5	6.5	7.5	94.48	91.63	64.35	61.03
9	85	5	6.5	15	96.82	86.63	59.84	61.01
10	85	5	10	7.5	97.43	102.59	77.07	77.68
11	85	1	6.5	15	91.66	98.21	56.13	57.15
12	70	3	3	7.5	94.14	91.60	51.85	52.71
13	85	3	10	15	96.44	98.25	67.71	69.24
14	85	3	10	0	67.17	62.22	16.85	16.17
15	85	1	10	7.5	87.55	84.79	66.65	66.46
16	85	3	6.5	7.5	95.93	96.34	76.49	68.39
17	100	3	10	7.5	98.00	101.66	79.59	81.41
18	85	3	6.5	7.5	96.58	96.34	67.38	68.39
19	70	3	6.5	0	31.87	40.87	2.54	5.37
20	85	3	6.5	7.5	96.88	96.34	74.42	68.39
21	70	3	10	7.5	89.33	84.37	62.64	59.54
22	100	5	6.5	7.5	98.22	102.27	78.11	71.02
23	85	5	6.5	0	85.15	81.72	15.85	17.50
24	100	3	6.5	0	87.96	81.42	14.83	16.52
25	85	3	3	15	97.50	96.84	49.43	46.64
26	85	3	3	0	77.10	69.67	9.64	4.64
27	85	3	6.5	7.5	96.61	96.34	62.68	68.39
28	100	3	3	7.5	94.37	102.46	48.34	54.11
29	85	5	3	7.5	97.69	102.91	56.30	57.28

removal efficiency. The optimum catalyst addition was 9%.

3.2.4. Effect of liquid-solid ratio on removal efficiency

Fig. 3(d) shows the effect of the liquid-solid ratio on the removal efficiency of nitrides and fluorides at a reaction temperature of 95 °C, reaction time of 3 h, and catalyst addition of 9%. As shown in Fig. 3(d), the removal efficiency of nitrides decreased first and then increased with the increment in liquid-solid ratio. When the liquid-solid ratio was 6 mL/g, the lowest removal efficiency of nitrides was 96.2%. Because there is a balance between the liquid-solid ratio and catalyst concentration, which promotes the removal efficiency of nitrides. Increasing the liquid-solid ratio and catalyst concentration can both promote the removal efficiency of nitrides. However, the concentration of catalyst decreased as the liquid-solid ratio increased. The removal efficiency of fluorides increased from 61.97% to 80.00% as the liquid-solid ratio increased from 3 mL/g to 7 mL/g then the removal efficiency decreased to 77%. The reason is that most fluorides are soluble fluoride salts and can be removed in a high liquid-solid ratio. However, when the liquid-solid ratio is greater than 7 mL/g, the concentration of fluorine reaches the concentration that reacts with sodium aluminate, and fluoride is converted into cryolite, resulting in a decrease in fluorine removal efficiency. The optimum liquid-solid ratio was 7 mL/g.

3.3. Response surface experiment

3.3.1. Analysis of response surface experimental results

Response surface experiments were performed based on single-factor experiments, and the results are shown in Table 3. The actual removal efficiency of nitrides ranged from 26.62% to 98.34%, and the calculated removal efficiency of nitrides ranged from 39.93% to 102.91%. The quadratic regression equation of the removal efficiency of nitrides is shown in Formula 4. The actual removal efficiency of fluorides ranged from 2.54% to 79.59%, and the calculated removal efficiency of fluorides ranged from 5.37% to 81.41%. The quadratic regression equation of the removal efficiency of fluorides is shown in Formula 5.

$$R_1 = -167.0489 + 1.53355A + 22.99322B - 7.17303C + 18.27176D - 0.10708AB + 0.040175AC - 0.11322AD + 0.19273BC - 0.88941BD + 0.084448CD - 0.012482A^2 - 0.78278B^2 + 0.16273C^2 - 0.29483D^2 \quad (4)$$

$$R_2 = -94.2257 + 2.05107A + 5.28618B - 1.64357C + 10.69514D - 0.027353AB + 0.097453AC + 0.00216376AD + 0.23805BC - 0.06763BD + 0.10542CD - 0.013123A^2 - 0.33826B^2 - 0.28511C^2 - 0.54616D^2 \quad (5)$$

Variances in the removal efficiency of nitrides and fluorides are exhibited in Tables 4 and 5, respectively. As shown in Table 4, the P values of A, B, D, AD, BD, and D^2 in the model were less than 0.05, which suggested that the linear effects of reaction temperature, reaction time, and catalyst addition on the removal efficiency of nitrides were significant. The interaction between reaction temperature and catalyst addition, as well as the interaction between reaction time and catalyst addition, had a significant influence on the removal efficiency of nitrides. The square of catalyst addition had a significant surface effect on the removal efficiency of nitrides. The P values of other parameters were greater than 0.05, which indicated that other factors had no significant effect on the removal efficiency of nitrides. The fitted values of F and P in the model were 7.82 and 0.0002, respectively, indicating that the model had remarkable adaptability.

In Table 5, the P values of A, B, C, D, and D^2 were less than 0.05, which suggested the linear effects of reaction temperature, reaction time, liquid-solid ratio, and catalyst addition on the removal efficiency of fluorides were significant. The square of catalyst addition had a significant surface effect on the removal efficiency of fluorides. The P values of other parameters were greater than 0.05, which indicated that other factors had no significant effect on the removal efficiency of fluorides. The fitted values of F and P in the model

Table 4
Analysis of variance table of removal efficiency of nitrides.

Source	Sum of Squares	df	Mean Square	F value	P value
Model	7802.38	14	557.31	7.82	0.0002
A	681.68	1	681.68	9.56	0.0080
B	684.86	1	684.86	9.61	0.0078
C	27.32	1	27.32	0.38	0.5458
D	2994.95	1	2994.95	42.02	<0.0001
AB	41.27	1	41.27	0.58	0.4593
AC	17.79	1	17.79	0.25	0.6251
AD	648.93	1	648.93	9.10	0.0092
BC	7.28	1	7.28	0.10	0.7540
BD	711.95	1	711.95	9.99	0.0069
CD	19.66	1	19.66	0.28	0.6077
A^2	51.16	1	51.16	0.72	0.4112
B^2	61.59	1	61.59	0.89	0.3609
C^2	25.78	1	25.78	0.36	0.5572
D^2	1784.05	1	1784.05	25.03	0.0002
Residual	997.93	14	71.28		
Lack of Fit	996.94	10	99.69		
Pure Error	0.99	4	0.25		
Cor Total	8800.31	28			

Table 5
Analysis of variance table of removal efficiency of fluorides.

Source	Sum of Squares	df	Mean Square	F value	P value
Model	14698.76	14	1049.91	41.31	<0.0001
A	406.1	1	406.1	16.75	0.0011
B	186.62	1	186.62	7.7	0.0149
C	871.93	1	871.93	36.05	<0.0001
D	6778.82	1	6778.82	279.66	<0.0001
AB	2.69	1	2.69	0.11	0.7438
AC	104.7	1	104.7	4.32	0.0565
AD	0.24	1	0.24	0.00978	0.9226
BC	11.11	1	11.11	0.46	0.5095
BD	4.12	1	4.12	0.17	0.6865
CD	30.63	1	30.63	1.26	0.2799
A^2	56.55	1	56.55	2.33	0.1489
B^2	11.87	1	11.87	0.49	0.4954
C^2	79.12	1	79.12	1.26	0.0923
D^2	6121.96	1	6121.96	252.57	<0.0001
Residual	339.35	14	24.24		
Lack of Fit	148.69	10	14.87		
Pure Error	190.66	4	47.66		
Cor Total	15038.11	28			

were 41.31 and < 0.0001, respectively, indicating that the model had remarkable adaptability.

3.3.2. Analysis of interaction between factors

Interactions were observed among the influential factors based on the single-factor experiment and variance analysis of the removal efficiency of nitrides and fluorides. The interaction among the factors that affect the removal efficiency of nitrides and fluorides must be discussed. The three-dimensional response surface map could visually show the influence of the two factors on the response value and determine the optimal range. The contour map reflected the interaction intensity of two factors and the effect on the response value. The ellipse contour line indicated that the interaction of two factors was obvious, and the closer the contour line was to the circle, the less obvious the interaction was [35].

3.3.2.1. Interaction of factors affecting removal efficiency of nitrides. A three-dimensional response surface map that indicated the effect of reaction temperature and catalyst addition on the removal of nitrides is exhibited in Fig. 4(a). The contour projection at the bottom was elliptical, indicating that the interaction between reaction temperature and catalyst addition was significant and had a substantial influence on the removal efficiency of nitrides. When the reaction time and liquid-solid ratio were 3 h and 6.5 mL/g, respectively, the removal efficiency of nitrides increased with the reaction temperature and catalyst addition. The color in the three-dimensional figure changed from blue to red, which represented an increase in the removal efficiency of nitrides. As shown in Fig. 4(b), the contour

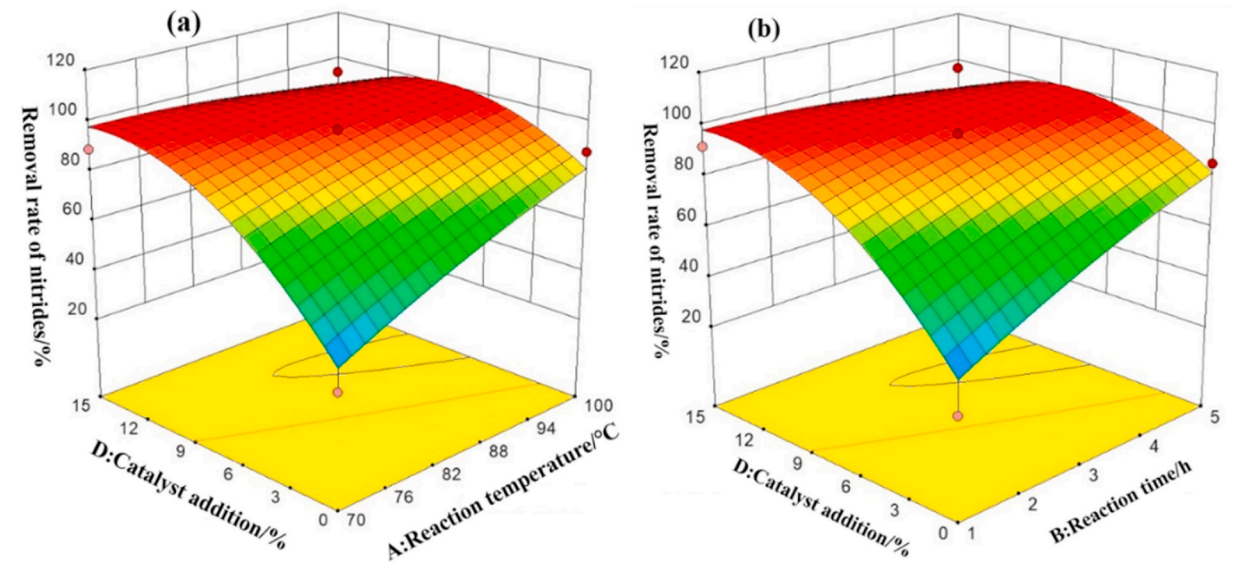

Fig. 4. Three-dimensional response surface maps: (a) Effect of A (reaction temperature)/D (catalyst addition) and (b) Effect of B (reaction time)/D (catalyst addition) on the removal of nitrides.

projection at the bottom was elliptical, indicating that the reaction time and catalyst addition interacted significantly with each other and had a significant influence on the removal efficiency of nitrides [26]. When the reaction temperature and liquid-solid ratio were 85 °C and 6.5 mL/g, the removal efficiency of nitrides increased with the reaction time and catalyst addition.

3.3.2.2. Interaction of factors that affect the removal efficiency of fluorides. As shown in Fig. 5, the contour projections of all the diagrams at the bottom were elliptical, indicating that the liquid-solid ratio and catalyst addition, reaction time and catalyst addition, and reaction temperature and catalyst addition interacted significantly. As shown in Fig. 5(a), when the reaction time and temperature were 3 h and 85 °C, respectively, the removal efficiency of fluorides increased with the increment in liquid-solid ratio. However, with the rising catalyst addition, the removal efficiency of fluorides first increased and then decreased. As shown in Fig. 5(b), when the reaction temperature and liquid-solid ratio were 85 °C and 6.5 mL/g, the removal efficiency of fluorides increased with the rising reaction time. Furthermore, with the rising catalyst addition, the removal efficiency of fluorides first increased and then decreased. As shown in Fig. 5 (c), when the reaction time and catalyst addition were 3 h and 6.5 mL/g, respectively, the removal efficiency of fluorides increased with the reaction temperature, and the removal efficiency of fluorides first increased and then decreased with the rising catalyst addition.

3.3.3. Results of response surface experiment

Based on variance analysis and three-dimensional response surface maps of removal efficiency of nitrides and fluorides, the optimum hydrolysis conditions, reaction temperature of 96.60 °C, reaction time of 2.85 h, liquid-solid ratio of 9.28 mL/g, and catalyst addition of 12.62% were obtained. Under optimum conditions, the removal efficiency of nitrides, the removal efficiency of fluorides,

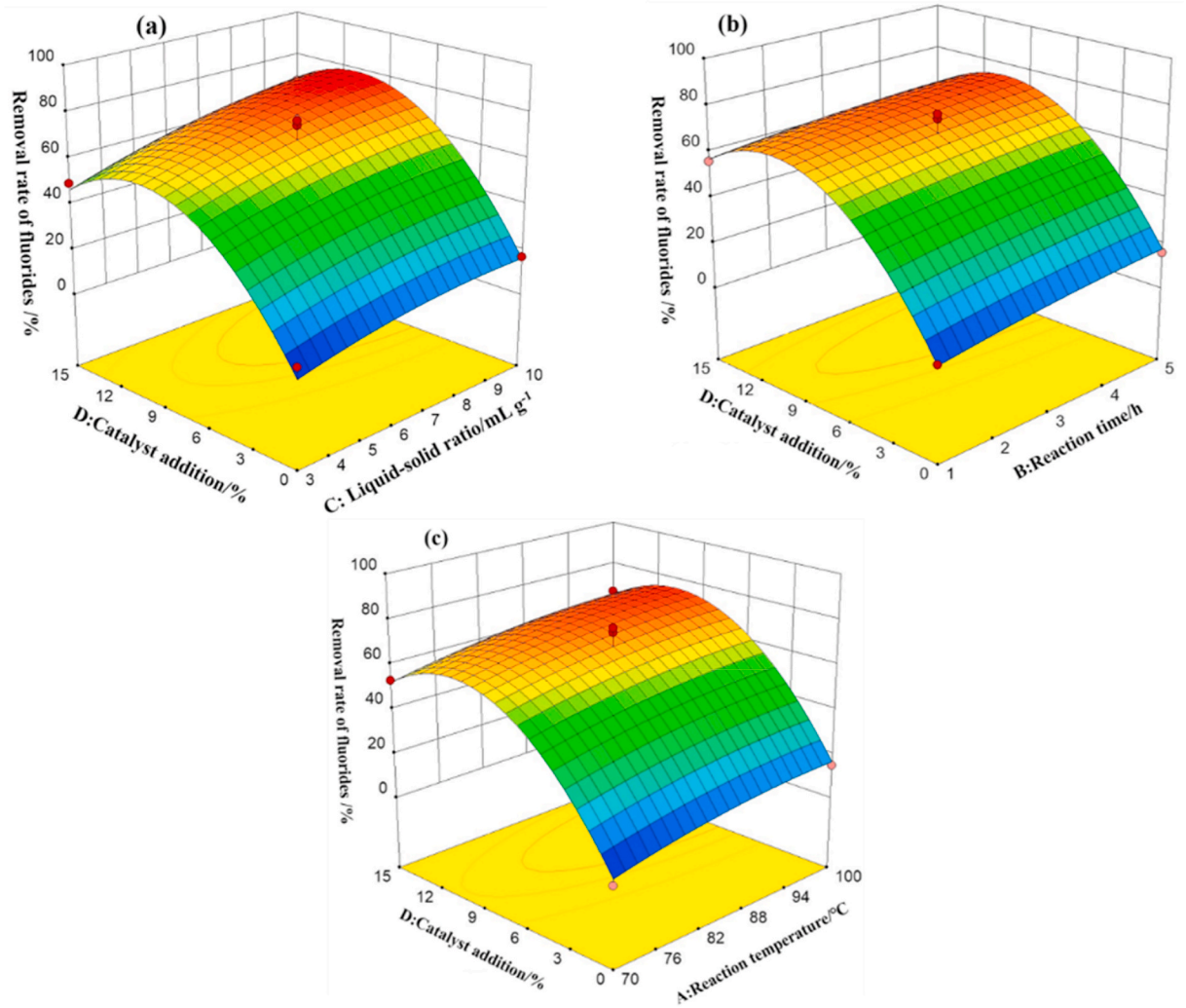

Fig. 5. Three-dimensional response surface maps (a) Effect of C (liquid-solid ratio)/D (catalyst addition), (b) Effect of B (reaction time)/D (catalyst addition), and (c) Effect of A (reaction temperature)/D (catalyst addition) on the removal of fluorides.

and the desirability of the model were 99.58%, 82.08%, and 1.00, respectively. The results were exhibited in Fig. 6.

According to optimum conditions, the experiment was performed, and the removal efficiencies of nitrides and fluorides were 99.03% and 81.93%, respectively. The experimental results were very close to the results predicted by the response surface model. The hydrolysis residues can be used to prepare PAC and ceramic materials. The hydrolysate is crystallized by evaporation to prepare the refining agent, which is returned to the ash frying system to recover aluminum.

3.4. Analysis of catalytic hydrolysis mechanism of SAD

3.4.1. Composition and phase analysis of hydrolysis residue

The hydrolysis residue was obtained from the catalytic hydrolysis of SAD under optimum experimental conditions. As shown in Table 6, the contents of Na, K, F, N, and Cl in the hydrolysis residue were 1.57%, 2.63%, 0.40%, 0.04%, and 0.21%, respectively, which were less than those in SAD. As shown in Fig. 7, the main phases in the hydrolysis residue were Al_2O_3 (PDF#88-0826), $MgAl_2O_4$ (PDF#78-1602), CaF_2 (PDF#77-2094), and $Al(OH)_3$ (PDF#77-0117). Compared with SAD, the phase of nitrides disappeared, and a new phase $Al(OH)_3$ was generated in the hydrolysis residue. Based on the XRF and XRD results, nitrides were converted into aluminum hydroxide and ammonia in the catalytic hydrolysis process, respectively. The soluble fluoride salts were dissolved. Identification for reactivity and extraction toxicity of hydrolysis residue were performed. As shown in Tables S1 and S2, the reaction activity and the extraction toxicity for hydrolysis residues both meet the concentration limits of GB5085.5-2007 and GB5085.3-2007, respectively.

3.4.2. Particle analysis of SAD and hydrolysis particle

Particle size change is an important basis for determining whether a reaction occurs [36]. To judge the catalytic hydrolysis degree of SAD, the particle size and pore diameter distribution in SAD and the hydrolysis residue were analyzed systematically. Fig. 8(a) shows the particle size distribution of SAD and hydrolysis residue. D_{50} decreased from 14.07 μm to 10.93 μm, and D_{90} decreased from 51.59 μm to 49.80 μm after catalytic hydrolysis. Fig. 8(b) and (c) show the N_2 adsorption and desorption isotherms and pore diameter distribution of the SAD and hydrolysis residue, respectively. N_2 adsorption and desorption curves of SAD and hydrolysis were the fourth type of isotherm, which was a type of mesoporous structure [37]. The hysteresis loop area of the SAD was smaller than that of the hydrolysis residue, which indicated that the porosity of the hydrolysis residue was larger than that of the SAD. The pore diameter distribution curve showed that the ratio of the SAD at a pore diameter of 2 nm was much lower than that of the hydrolysis residue. The surface area of particles in the catalytic hydrolysis process changed from 5.086 m^2/g to 30.253 m^2/g. Combining particle size, pore diameter distribution, and surface area analysis, catalytic hydrolysis did not cause the SAD particles to be destroyed completely, only fluoride and chlorine salts were shed, thereby forming pores. Furthermore, the aluminum hydroxide generated in the catalyzed hydrolysis process occupied the position of nitrides.

3.4.3. Transformation rule of fluorides and nitride

To confirm the change in the chemical structure of fluorides and nitrides in the catalytic hydrolysis process, the FTIR spectra of the SAD and hydrolysis residue are shown in Fig. 9. Compared with the SAD, a series of stronger intensity absorption peaks existed in the hydrolysis residue at approximately 3400, 2100 and 1640 cm^{-1}, which were attributable to $Al(OH)_3$ [38]. The peak at approximately 2100 cm^{-1} was attributable to the O–H stretching vibration of AlOH. The peak positioned at approximately 1200 cm^{-1}, which was the characteristic peak of AlN [38], disappeared after the catalytic hydrolysis. The absorption peaks at 1398, 710, and 570 cm^{-1} were both found in SAD and hydrolysis residue. The peaks positioned at 1398, 710 and 570 cm^{-1} were attributed to α-Al_2O_3, AlN and γ-Al_2O_3, respectively [39]. However, the absorption peak at 710 cm^{-1} in hydrolysis was much weaker than that in SAD. It suggested that AlN reacted but α-Al_2O_3 and γ-Al_2O_3 did not react in catalyst hydrolysis. The FTIR spectra suggested that AlN was transformed to $Al(OH)_3$.

The SEM and element surface distribution of the SAD and hydrolysis residue were investigated. As shown in Fig. 10, AlN existed in the SAD, and fluorite bonded with potassium and calcium and formed potassium fluorides and calcium fluorides. After the catalytic hydrolysis reaction, the morphology of fluorine and AlN changed significantly. As shown in Fig. 11, the signal for nitrogen element was

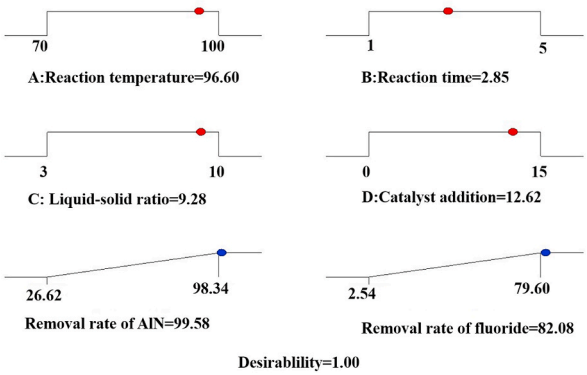

Fig. 6. Satisfaction slope function graph.

Table 6
Chemical composition of hydrolysis residue (wt. %).

Al	Mg	Na	K	Si	Ca	N	S	Fe	Mn	Se	O	Ti	F	Cl
40.09	6.28	1.57	2.63	0.92	0.79	0.04	0.30	0.43	0.32	0.27	45.64	0.11	0.40	0.21

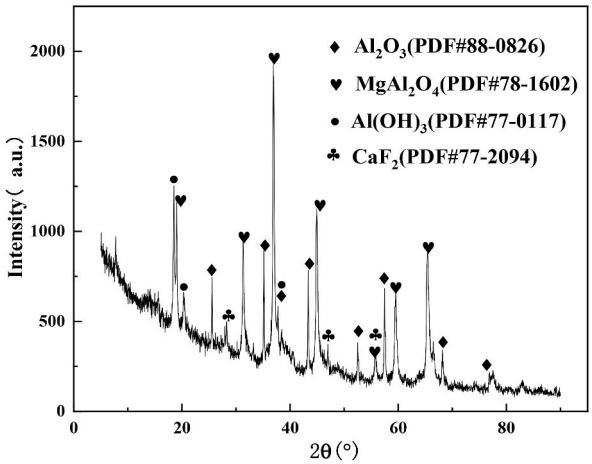

Fig. 7. XRD pattern of hydrolysis residue.

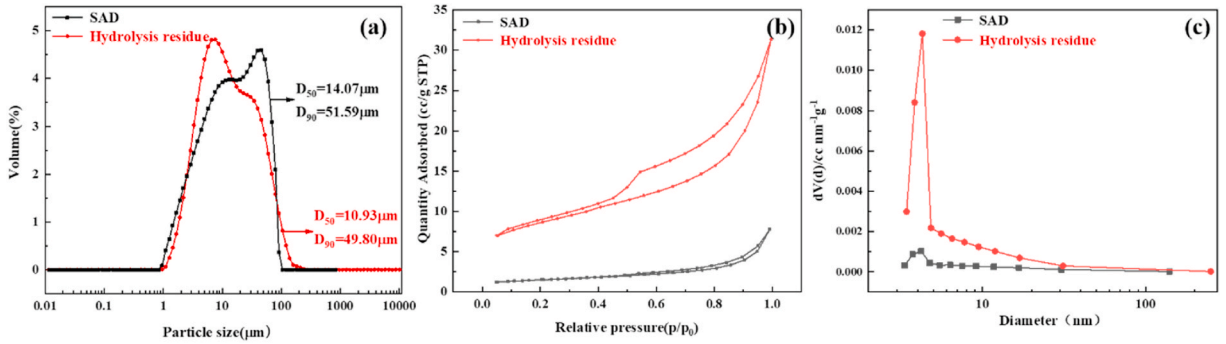

Fig. 8. (a) Particle size distribution; (b) Nitrogen adsorption-desorption isotherms; (c) Pore diameter distribution of SAD and hydrolysis residue.

weak at the location of aluminum element. And the signal for fluoride element was also weak at the location of potassium element. The results suggested some AlN and KF were removed combining XRD and XRF analysis. Whereas the signal for fluorine was strong at the location of calcium element. This suggested that CaF_2 was still present in the hydrolysis residue.

To further confirm the transformation rule of fluorides and nitrides, the SAD and hydrolysis residue were examined by XPS. As shown in Fig. 12(a), the chemical forms of aluminum in SAD were Al–O–Mg, Al–N and Al–O with the binding energy at 74.55, 74.01, and 74.71 eV, respectively [28]. According to the integral area calculation, the relative contents of Al–O–Mg, Al–N and Al–O were 67.57%, 6.76%, and 25.68%, respectively. While the chemical forms of aluminum were Al–O–Mg, Al–OH and Al–O in hydrolysis residue. According to XRD analysis, AlN was hydrolyzed to $Al(OH)_3$. As shown in Fig. 12(b), there is one strong peak of Ca–F at 685.6 eV in SAD. And there are two peaks of Ca–F at 685.6 eV and 688.97 eV in hydrolysis residue, respectively [40]. However, the peak intensity of Ca–F in hydrolysis residue is much weaker than that of SAD. K–F and Na–F were not detected because the content of KF and NaF did not meet the minimum test line for XPS.

The process of catalytic hydrolysis was investigated systematically. As shown in Fig. 13(a), the SAD particles were wrapped around each other. It was easy for the AlN and solution fluorides on the surface of the SAD particles to react with water and dissolve. However, $Al(OH)_3$ was formed after hydrolysis of AlN. The insoluble $Al(OH)_3$ could cover AlN, which restrict hydrolysis of AlN. When the catalyst was additive into liquids, $Al(OH)_3$ was reactive with catalyst NaOH to promote hydrolysis of AlN. As shown in Fig. 13(b), ammonia is easy to spill out in alkaline environment, and the chemical equilibrium movement promotes the hydrolysis reaction of aluminum nitride. This will help to form pores in the SAD particles. The pores would help water enter the center of the SAD particles to promote the removal of nitrides and fluorides thoroughly.

In the hydrolysis process, chemical reactions, such as Formulas (6)−(13), occurs. AlN reacts with water to form $Al(OH)_3$ and NH_3.

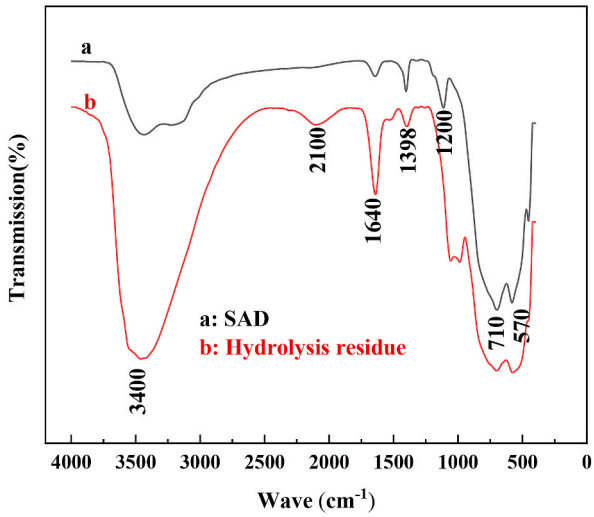

Fig. 9. FTIR spectra of SAD and hydrolysis residue.

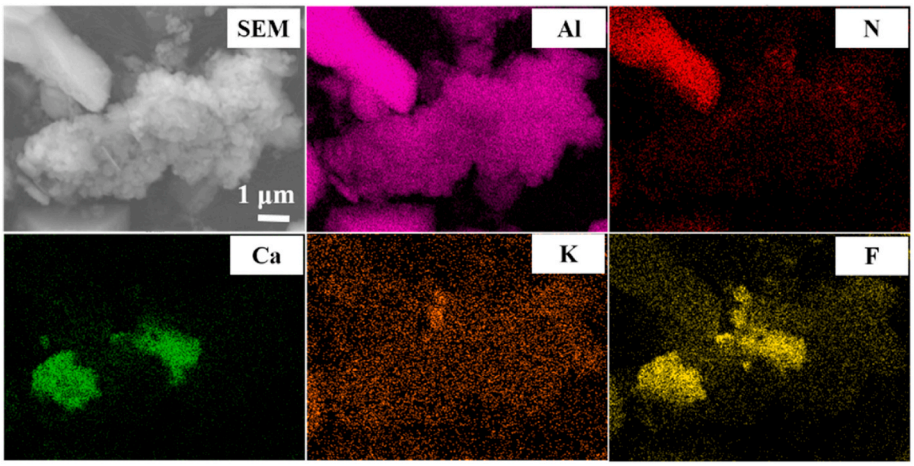

Fig. 10. SEM and element surface distribution of SAD.

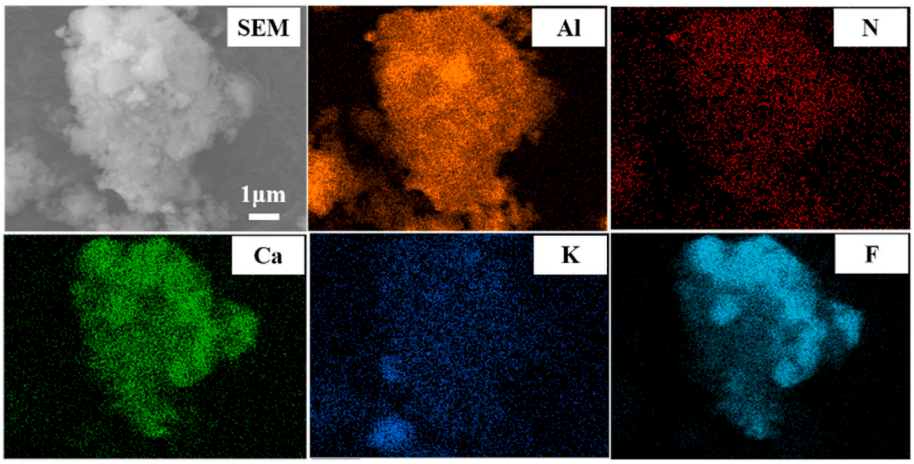

Fig. 11. SEM and element surface distribution of hydrolysis residue.

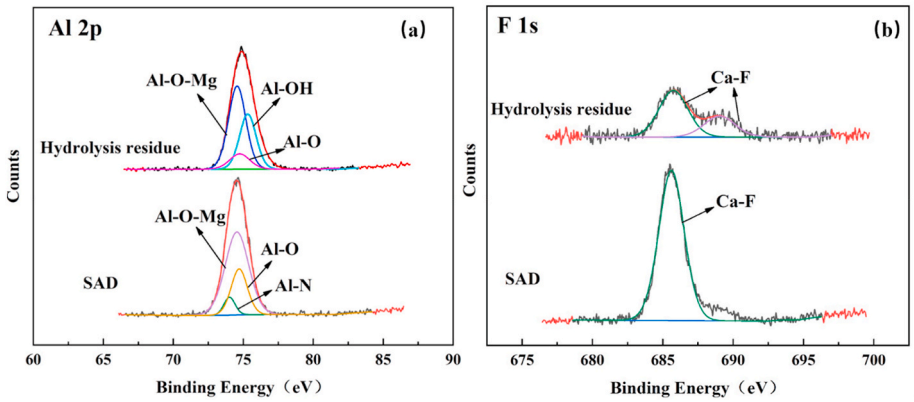

Fig. 12. (a) Al 2p and (b) F 1s peaks of SAD and hydrolysis residue by XPS analysis.

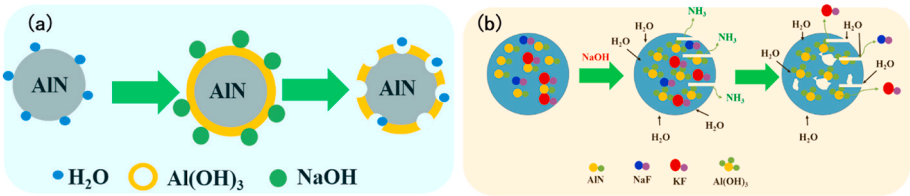

Fig. 13. (a) Catalyst hydrolysis of AlN; (b) Nitrides and fluorides removal from SAD.

Then, NH_3 is easily soluble in water to form $NH_3{\cdot}H_2O$. However, many other anions, such as F^- and Cl^-, are dissolved from SAD in the solution, thereby promoting $NH_3{\cdot}H_2O$ conversion into NH_4Cl or NH_4F. Converting to NH_3 escaping from reactors is difficult for NH_4Cl and NH_4F. Therefore, the high-concentration ammonia system in the reactors inhibited the hydrolysis of AlN. When NaOH catalyst is added, NaOH reacts with $Al(OH)_3$ covering the surface of AlN to promote hydrolysis of AlN. It is easy for NH_3 to escape from the reactors in alkaline solution. It will promote the hydrolysis of AlN by chemical equilibrium. The hydrolysis of AlN destroyed the particles of SAD to promote the dissolution of the coated fluorides into the liquid. However, there is a secondary reaction that NaF and NH_4F conversion to Na_3AlF_6, NH_3 and H_2O in $NaAlO_2$ solution. It is bad for removal of fluorides. So the reaction conditions must be controlled strictly.

$$AlN + 3H_2O \rightarrow Al(OH)_3 + NH_3\uparrow \tag{6}$$

$$Al(OH)_3 + NaOH \rightarrow NaAlO_2 + 2H_2O \tag{7}$$

$$NH_3 + H_2O \rightleftharpoons NH_3 \cdot H_2O \tag{8}$$

$$NH_3 \cdot H_2O \rightleftharpoons NH_4^+ + OH^- \tag{9}$$

$$(K, Na)F \rightarrow K^+ + Na^+ + F^- \tag{10}$$

$$NH_3{\cdot}H_2O + Cl^- + F^- \rightarrow NH_4(Cl, F) + OH^- \tag{11}$$

$$NH_4(Cl, F) + OH^- \xrightarrow{NaOH} NH_4OH + Cl^- + F^- \tag{12}$$

$$2NaF + 4NH_4F + NaAlO_2 \rightarrow Na_3AlF_6 \downarrow + 4NH_3 \uparrow + 2H_2O \tag{13}$$

4. Conclusions

This paper realizes the efficient and simultaneous removal of nitrides and fluorides. In addition, the mechanism of catalytic hydrolysis removal of nitrides and fluorides from SAD is illustrated clearly. The results are detailed as follows:

(1) The optimum hydrolysis conditions, reaction temperature of 96.60 °C, reaction time of 2.85 h, liquid-solid ratio of 9.28 mL/g, and catalyst addition of 12.62% were obtained. Under optimum conditions, the removal efficiencies of nitrides and fluorides reached 99.03% and 81.93%, respectively.

(2) The mechanism of nitride removal is that AlN is hydrolyzed to $Al(OH)_3$ and NH_3. Moreover, the catalyst of NaOH reacts with $Al(OH)_3$ covering the surface of AlN and promotes the escape of NH_3 from reactors to accelerate the hydrolysis of AlN and remove nitrides thoroughly.
(3) In the catalytic hydrolysis process, the average diameters of particles decreased from 14.07 μm to 10.93 μm, the specific surface area of particles increased from 5.086 m^2/g to 30.253 m^2/g, and the porosity of hydrolysis residues was 12 times higher than those of SAD. The mechanism of fluoride removal is that the hydrolysis of AlN makes SAD particles porous to promote fluoride coating to dissolve into liquid. The removal of nitrides and fluorides was a synergistic process.

Author contribution statement

Zhanbing Li: Performed the experiments; Analyzed and interpreted the data; Wrote the paper.
Huiquan Li: Conceived and designed the experiments; Analyzed and interpreted the data.
Xingzhong Huang: Performed the experiments; Contributed reagents, materials, analysis tools or data.
Wenfen Wu; Zhenhua Sun: Analyzed and interpreted the data.
Xiuwen Wu; Shaopeng Li: Conceived and designed the experiments.

Funding statement

Zhanbing Li was supported by National Key Research and Development Program, China [2018YFC1901906].
Huiquan Li was supported by Key Research and Development Program (Major Science and Technology Innovation Project) of Shandong, China [2019JZZY010504].

Data availability statement

Data included in article/supp. material/referenced in article.

Declaration of interest's statement

The authors declare no competing interests.

Abbreviations

SAD	Secondary aluminum dross
PAC	Polyaluminum chloride
SAD	Secondary aluminum dross
PAC	Polyaluminum chloride
XRF	X-ray fluorescence spectrometry
XRD	X-ray diffractometry
SEM	scanning electron microscopy
FTIR	Fourier infrared spectroscopy
XPS	X-ray photoelectron spectroscopy

Appendix B. Supplementary data

Supplementary data related to this article can be found at https://doi.org/10.1016/j.heliyon.2023.e12893.

References

[1] J. Hong, J. Wang, H. Chen, B. Sun, J. Li, C. Chen, Process of aluminum dross recycling and life cycle assessment for Al-Si alloys and brown fused alumina, Trans. Nonferrous Metals Soc. China 20 (2010) 2155–2161, https://doi.org/10.1016/S1003-6326 (09) 60435-0.
[2] D. Brough, H. Jouhara, The aluminium industry: a review on state-of-the-art technologies, environmental impacts and possibilities for waste heat recovery, Int. J. Thermofluids 1–2 (2020), 100007, https://doi.org/10.1016/j.ijft.2019.100007.
[3] H. Shen, B. Liu, C. Ekberg, S. Zhang, Harmless disposal and resource utilization for secondary aluminum dross: a review, Sci. Total Environ. 760 (2021), 143968, https://doi.org/10.1016/j.scitotenv.2020.143968.
[4] A. Meshram, K.K. Singh, Recovery of valuable products from hazardous aluminum dross: a review, Resour. Conserv. Recycl. 130 (2018) 95–108, https://doi.org/10.1016/j.resconrec.2017.11.026.
[5] M. Mahinroosta, A. Allahverdi, Hazardous aluminum dross characterization and recycling strategies: a critical review, J. Environ. Manag. 223 (2018) 452–468, https://doi.org/10.1016/j.jenvman.2018.06.068.
[6] P.E. Tsakiridis, P. Oustadakis, S. Agatzini-Leonardou, Aluminum recovery during black dross hydrothermal treatment, J. Environ. Chem. Eng. 1 (2013) 23–32, https://doi.org/10.1016/j.jece.2013.03.004.
[7] Y. Zhang, Z. Guo, Z. Han, X. Xiao, Effect of rare earth oxides doping on MgAl2O4 spinel obtained by sintering of secondary aluminum dross, J. Alloys Compd. 735 (2018) 2597–2603, https://doi.org/10.1016/j.jallcom.2017.11.356.

[8] A. Li, H. Zhang, H. Yang, Evaluation of aluminum dross as raw material for high-alumina refractory, Ceram. Int. 40 (2014) 12585–12590, https://doi.org/10.1016/j.ceramint.2014.04.069.

[9] D. Wang, C. Xue, Y. Cao, J. Zhao, Microstructure design and preparation of Al2O3/TiC/TiN micro-nano-composite ceramic tool materials based on properties prediction with finite element method, Ceram. Int. 44 (2018) 5093–5101, https://doi.org/10.1016/j.ceramint.2017.12.109.

[10] C.T. Foo, M.A.M. Salleh, K.K. Ying, K.A. Matori, Mineralogy and thermal expansion study of mullite-based ceramics synthesized from coal fly ash and aluminum dross industrial wastes, Ceram. Int. 45 (2019) 7488–7494, https://doi.org/10.1016/j.ceramint.2019.01.041.

[11] M.H.A. Aziz, M.H.D. Othman, N.A. Hashim, M.A. Rahman, J. Jaafar, S.K. Hubadillah, Z.S. Tai, Pretreated aluminum dross waste as a source of inexpensive alumina-spinel composite ceramic hollow fibre membrane for pretreatment of oily saline produced water, Ceram. Int. 45 (2019) 2069–2078, https://doi.org/10.1016/j.ceramint.2018.10.110.

[12] A. López-Delgado, J.I. Robla, I. Padilla, S. López-Andrés, M. Romero, Zero-waste process for the transformation of a hazardous aluminum waste into a raw material to obtain zeolites, J. Clean. Prod. 255 (2020) 120178, https://doi.org/10.1016/j.jclepro.2020.120178.

[13] E. David, J. Kopac, Aluminum recovery as a product with high added value using aluminum hazardous waste, J. Hazard Mater. 261 (2013) 316–324, https://doi.org/10.1016/j.jhazmat.2013.07.042.

[14] B.R. Das, B. Dash, B.C. Tripathy, I.N. Bhattacharya, S.C. Das, Production of η-alumina from waste aluminum dross, Miner. Eng. 20 (2007) 252–258, https://doi.org/10.1016/j.mineng.2006.09.002.

[15] A. Meshram, D. Gautam, A. Jain, M.D. Rao, D. Mohan, K.K. Singh, Employing organic solvent precipitation to produce tamarugite from white aluminum dross, J. Clean. Prod. 231 (2019) 835–845, https://doi.org/10.1016/j.jclepro.2019.05.269.

[16] A. Meshram, A. Jain, D. Gautam, K.K. Singh, Synthesis and characterization of tamarugite from aluminum dross: Part I, J. Environ. Manag. 232 (2019) 978–984, https://doi.org/10.1016/j.jenvman.2018.12.019.

[17] N. Murayama, N. Okajima, S. Yamaoka, H. Yamamoto, J. Shibata, Hydrothermal synthesis of AlPO4-5 type zeolitic materials by using aluminum dross as a raw material, J. Eur. Ceram. Soc. 26 (2006) 459–462, https://doi.org/10.1016/j.jeurceramsoc.2005.06.022.

[18] Y. Liu, B.S. Leong, Z.-T. Hu, E.-H. Yang, Autoclaved aerated concrete incorporating waste aluminum dust as foaming agent, Construct. Build. Mater. 148 (2017) 140–147, https://doi.org/10.1016/j.conbuildmat.2017.05.047.

[19] E.M.M. Ewais, N.M. Khalil, M.S. Amin, Y.M.Z. Ahmed, M.A. Barakat, Utilization of aluminum sludge and aluminum slag (dross) for the manufacture of calcium aluminate cement, Ceram. Int. 35 (2009) 3381–3388, https://doi.org/10.1016/j.ceramint.2009.06.008.

[20] E. David, J. Kopac, Hydrolysis of aluminum dross material to achieve zero hazardous waste, J. Hazard Mater. 209–210 (2012) 501–509, https://doi.org/10.1016/j.jhazmat.2012.01.064.

[21] M. Mahinroosta, A. Allahverdi, A promising green process for synthesis of high purity activated-alumina nanopowder from secondary aluminum dross, J. Clean. Prod. 179 (2018) 93–102, https://doi.org/10.1016/j.jclepro.2018.01.079.

[22] M. Mahinroosta, A. Allahverdi, Enhanced alumina recovery from secondary aluminum dross for high purity nanostructured γ-alumina powder production: kinetic study, J. Environ. Manag. 212 (2018) 278–291, https://doi.org/10.1016/j.jenvman.2018.02.009.

[23] M. Mahinroosta, A. Allahverdi, P. Dong, N. Bassim, Green template-free synthesis and characterization of mesoporous alumina as a high value-added product in aluminum black dross recycling strategy, J. Alloys Compd. 792 (2019) 161–169, https://doi.org/10.1016/j.jallcom.2019.04.009.

[24] N. Murayama, I. Maekawa, H. Ushiro, T. Miyoshi, J. Shibata, M. Valix, Synthesis of various layered double hydroxides using aluminum dross generated in aluminum recycling process, Int. J. Miner. Process. 110–111 (2012) 46–52, https://doi.org/10.1016/j.minpro.2012.03.011.

[25] X. Zhao, Y. Liu, G. Lyu, Y. Zhang, T. Zhang, Removal of fluorine, chlorine, and nitrogen from aluminum dross by wet process, in: D. Eskin (Ed.), Light Met. 2022, Springer International Publishing, Cham, 2022, pp. 48–55, https://doi.org/10.1007/978-3-030-92529-1_7.

[26] S. Lv, H. Ni, X. Wang, W. Ni, W. Wu, Effects of hydrolysis parameters on AlN content in aluminum dross and multivariate nonlinear regression analysis, Coatings 12 (2022) 552, https://doi.org/10.3390/coatings12050552.

[27] Q. Li, Q. Yang, G. Zhang, Q. Shi, Investigations on the hydrolysis behavior of AlN in the leaching process of secondary aluminum dross, Hydrometallurgy 182 (2018) 121–127, https://doi.org/10.1016/j.hydromet.2018.10.015.

[28] Y. Li, Z. Qin, C. Li, Y. Qu, H. Wang, L. Peng, Y. Wang, Hazardous characteristics and transformation mechanism in hydrometallurgical disposing strategy of secondary aluminum dross, J. Environ. Chem. Eng. 9 (2021), 106470, https://doi.org/10.1016/j.jece.2021.106470.

[29] J. Tang, G. Liu, T. Qi, Q. Zhou, Z. Peng, X. Li, H. Yan, H. Hao, Two-stage process for the safe utilization of secondary aluminum dross in combination with the Bayer process, Hydrometallurgy (2022), https://doi.org/10.1016/j.hydromet.2022.105836.

[30] Q. Gao, Q. Guo, Y. Li, B. Ren, M. Fu, H. Li, D. Tian, M. Ding, Innovative technology for defluorination of secondary aluminum dross by alkali leaching, Miner. Eng. 172 (2021), 107134, https://doi.org/10.1016/j.mineng.2021.107134.

[31] H. Lv, H. Zhao, Z. Zuo, R. Li, F. Liu, A thermodynamic and kinetic study of catalyzed hydrolysis of aluminum nitride in secondary aluminum dross, J. Mater. Res. Technol. 9 (2020) 9735–9745, https://doi.org/10.1016/j.jmrt.2020.06.051.

[32] F. Liu, Z. Zuo, J. Han, H. Zhao, R. Li, Removal process and kinetics of nitrogen and chlorine removal from black aluminum dross, J. Sustain. Metall. 7 (2021) 1805–1818, https://doi.org/10.1007/s40831-021-00461-0.

[33] X. Zhu, J. Yang, Y. Yang, Q. Huang, T. Liu, Pyrometallurgical process and multipollutant co-conversion for secondary aluminum dross: a review, J. Mater. Res. Technol. 21 (2022) 1196–1211, https://doi.org/10.1016/j.jmrt.2022.09.089.

[34] M. Kadotani, S. Isobe, Process for the Production of High Quality Synthetic Cryolite [P]. US3656894D, 1972.

[35] J. Shi, Efficiency and Mechanisms for the Removal of Ciprofloxacin in Water by Red Mud and its Modification, Doctor, Xi'an University of Technology, 2020.

[36] J. Zhang, S. Li, H. Li, Q. Wu, X. Xi, Z. Li, Preparation of Al–Si composite from high-alumina coal fly ash by mechanical–chemical synergistic activation, Ceram. Int. 43 (2017) 6532–6541, https://doi.org/10.1016/j.ceramint.2017.02.075.

[37] K.S.W. Sing, Reporting physisorption data for gas/solid systems with special reference to the determination of surface area and porosity (Recommendations 1984), Pure Appl. Chem. 57 (1985) 603–619, https://doi.org/10.1351/pac198557040603.

[38] Y. Zhang, J. Binner, Hydrolysis process of a surface treated aluminum nitride powder—a FTIR study, J. Mater. Sci. Lett. 21 (2002) 803–805, https://doi.org/10.1023/A:1015714212305.

[39] J. Gangwar, B.K. Gupta, S.K. Tripathi, A.K. Srivastava, Phase dependent thermal and spectroscopic responses of Al2O3 nanostructures with different morphogenesis, Nanoscale 7 (2015) 13313–13344, https://doi.org/10.1039/C5NR02369F.

[40] J. Moulder, William F. Stickle, P.E. Sobol, K.D. Bomben, Handbook of X-Ray Photoelectron Spectroscopy: a Reference Book of Standard Spectra for Identification and Interpretation of XPS Data, Perkin-Elmer Corporation, 1979, 55344.